

Single Dirac cone with a flat band touching on line-centered-square optical lattices

R. Shen,* L. B. Shao, Baigeng Wang, and D. Y. Xing

National Laboratory of Solid State Microstructures and Department of Physics, Nanjing University, Nanjing, 210093 China

(Received 31 July 2009; published 14 January 2010)

Using ultracold atoms trapped in an optical lattice, we form a line-centered-square lattice in the condensed-matter physics, where a crossover from massive to massless Dirac fermion behavior can be easily achieved by tuning the laser intensities. The present Dirac fermions satisfy a three-component quantum equation for pseudospin-1 fermions, resulting in a single Dirac cone in the energy spectrum, a flat band touching at the Dirac point, and a vanishing Berry's phase. Interestingly, the massless Dirac fermions here may exhibit an all-angle Klein tunneling; i.e., the barrier is completely transparent for all incident angles.

DOI: 10.1103/PhysRevB.81.041410

PACS number(s): 73.20.-r, 05.30.Fk

In the last few years, a variety of two-dimensional atomic crystals had been prepared,¹ among which graphene has attracted considerable attention due to the Dirac cone structure in its electronic energy spectrum.²⁻⁶ There are two inequivalent Dirac points in graphene, and a π Berry's phase is acquired for the particles circling each of them.⁷ The conduction band and the valence band of graphene touch each other at two Dirac points. In the vicinity of the Dirac points the energy disperses linearly in the wave vector, which resembles the spectrum of the relativistic particles. In conventional two-dimensional electron systems, such as graphene, the Dirac points must come in pairs.⁸ Recently, the appearance of the single Dirac cone structure in the surface states of the three-dimensional strong topological insulators has aroused particular interest.⁹⁻¹³ The nontrivial Z_2 invariants in the strong topological insulators imply the existence of gapless surface states and the surface states form a two-dimensional "topological metal" in which the Fermi arc encloses an odd number of Dirac points with π Berry's phase.^{9,10}

With present-day technology, the ultracold atoms can be confined in a gauge potential created by interfering optical laser beams to form an artificial crystal of light.¹⁴ Since the interaction strength can be easily controlled and artificial magnetic fields can be created, ultracold atom systems provide a clean environment to study the complex physics in the condensed matter in a controllable fashion.¹⁴⁻¹⁹ For example, ultracold atoms can be used to simulate the Mott-Hubbard transition,²⁰ the fractional quantum Hall effect,²¹ the spin Hall effect,²² and the spin field effect transistors.²³ The massless Dirac fermions are also simulated by the ultracold atoms in the honeycomb optical lattice.²⁴

In this Rapid Communication, we present a type of two-dimensional example for the massless Dirac fermions, which is topologically different from those reported previously. Using ultracold atoms trapped in an optical lattice, we form a line-centered-square (LCS) lattice in the condensed-matter physics, where a crossover from massive to massless Dirac fermion behavior can be easily achieved by tuning the laser intensities. Interestingly, there is only a single Dirac cone in the energy spectrum accompanied by the flat band touching at the Dirac point. The touching between the flat and the dispersive band is protected by the real-space topology as in the kagome, dice, pyrochlore, and honeycomb p -band models.^{25,26} The occurrence of the single Dirac cone here is

completely different from those reported in the surface states of the three-dimensional strong topological insulators. The single Dirac cone on the LCS lattice stems from the fact that the present Dirac fermions do not satisfy the two-component Weyl equation but a three-component quantum equation for pseudospin-1 fermions, which also results in a vanishing Berry's phase enclosing the Dirac point and unique Landau levels. In addition, the massless Dirac fermions on the LCS lattice are found to exhibit an unimpeded penetration through high and wide potential barriers, similar to the Klein tunneling in graphene.²⁷ More strikingly, the present Klein tunneling could be all angle; i.e., the barrier is completely transparent for all incident angles.

The LCS lattice is schematically illustrated in Fig. 1(a). There are three sublattices denoted by the black, red, and green points, respectively. All sites A (black points) form a standard square lattice. Sites B (red points) and C (green points) are located at the bond centers of sublattice A , forming the other two square lattices. The LCS lattice is the two-dimensional counterpart of the face-centered-cubic lattice and can be realized in the ultracold atomic system as below.

Consider an assembly of single-component ultracold fer-

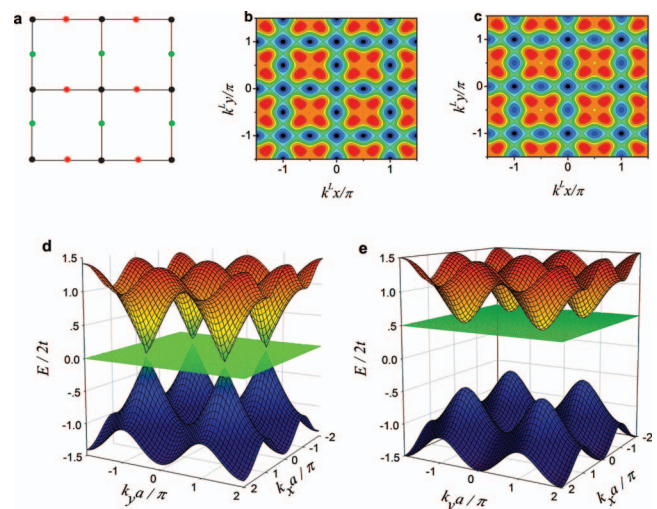


FIG. 1. (Color) (a) Schematic illustration of the LCS lattice, energy contour of the optical potential in Eq. (1) with (b) $V_1=2V_2$ and (c) $V_1=2.2V_2$, and dispersion relation on the LCS lattice with (d) $\Delta=0$ and (e) $\Delta=t$.

mionic atoms, such as ^{40}K and ^6Li . In order to avoid the interaction between the different spin components of those atoms one needs to introduce a magnetic field that freezes the spin. The effectively two-dimensional system can be realized by raising the potential barrier of the optical lattice along the z direction to suppress the vertical tunneling between different planes. In the x - y plane, a detuned standing-wave laser beam creates the optical potential in the form of $V \sin^2(\mathbf{k}^L \cdot \mathbf{r} + \varphi)$, where V is the potential amplitude, \mathbf{k}^L is the optical wave vector, φ is the phase of the laser beam, and \mathbf{r} is the coordinate vector. In order to generate the LCS optical lattice, we apply six detuned standing-wave laser beams. Four of them are applied along the \mathbf{e}_x and \mathbf{e}_y directions with optical wave vectors k^L and $2k^L$, respectively. Two of them are applied along the $(\mathbf{e}_x \pm \mathbf{e}_y)/\sqrt{2}$ directions with optical wave vector $\sqrt{2}k^L$ and relative phase $\pi/2$, respectively. The resulting optical potential is given by

$$V(x,y) = V_1(\sin^2 k^L x + \sin^2 k^L y + \sin^2 2k^L x + \sin^2 2k^L y) + V_2 \left(\sin^2 \left[k^L(x+y) + \frac{\pi}{2} \right] + \sin^2 \left[k^L(x-y) + \frac{\pi}{2} \right] \right), \quad (1)$$

where potential amplitudes V_1 and V_2 can be easily tuned by varying the laser intensities along different directions. The Energy contours of optical potential $V(x,y)$ are plotted in Fig. 1(b) for $V_1=2V_2$ and Fig. 1(c) for $V_1=2.2V_2$, in which the potential minima are marked with the black and blue points. The atoms are trapped at those minima, forming the LCS lattice with lattice constant $a=\pi/k^L$. For $V_1=2V_2$, $V(x,y)$ is the same at sites $A-C$ so that their site energies ε_A , ε_B , and ε_C are expected to be the same. If $V_1 \neq 2V_2$, we have $\varepsilon_B=\varepsilon_C$, but different from ε_A . For instance, the site energy at sites B and C marked with blue points is higher than that at sites A with black points in Fig. 1(c). Therefore, the LCS lattice can be created in the ultracold atomic system and the site energies of different sublattices can be easily controlled.

For single-component fermionic atoms, the nearest-neighbor tight-binding Hamiltonian on the LCS lattice is given by $H_0 = \sum_i \varepsilon_i c_i^\dagger c_i - t \sum_{\langle i,j \rangle} c_i^\dagger c_j$, where $\langle i,j \rangle$ denotes the nearest-neighboring sites and t is the hopping constant. Due to the symmetry consideration, the site energies are set as $\varepsilon_B=\varepsilon_C=-\varepsilon_A=\Delta$. For sublattice X with $X=A-C$, one can define three Bloch sums, $|kX\rangle = (1/\sqrt{N}) \sum_{i \in X} e^{ik \cdot \mathbf{r}_i} c_i^\dagger |0\rangle$, where \mathbf{k} is the wave vector in the Brillouin zone, and the summation of i goes over all sites X . Taking the three Bloch sums as the bases, the Hamiltonian can be written as

$$H_0 = \begin{pmatrix} \Delta & -2t \cos(k_x a/2) & 0 \\ -2t \cos(k_x a/2) & -\Delta & -2t \cos(k_y a/2) \\ 0 & -2t \cos(k_y a/2) & \Delta \end{pmatrix}, \quad (2)$$

in the 3×3 matrix form. After the diagonalization, the energy eigenvalues are obtained as three branches. One is a flat band with energy $E_0=\Delta$. The other two dispersive bands are $E_{\pm} = \pm \sqrt{\Delta^2 + 4t^2 [\cos^2(k_x a/2) + \cos^2(k_y a/2)]}$. The dispersion relations are plotted in Fig. 1(d) for $\Delta=0$ and Fig. 1(e) for $\Delta=t$.

A most important feature in the band structure of the LCS lattice is the presence of the flat band, which is completely dispersionless in the whole Brillouin zone. The states in the flat band is localized as a result of destructive interference.²⁶ The models with the flat band are of particular interest in strongly correlated electron systems. In reality, the fractional quantum Hall effect occurs as a result of the flat-band degeneracy of Landau levels of electrons in a magnetic field. The flat band is a powerful mechanism for generating the interesting many-body states, the interaction reconstructing the states within the flat-band manifold without any cost in the kinetic energy.²⁶ At $\Delta=0$ ($\varepsilon_B=\varepsilon_C=\varepsilon_A$), the two dispersive bands touch at point R of the Brillouin zone with $\mathbf{k}_R = (\pi/a, \pi/a)$, and the flat band also touches both of them, as shown in Fig. 1(d). Around the touching point, there appears a Dirac cone structure, which is similar to that in graphene. For positive (negative) Δ , the flat band only touches the upper (lower) dispersive band at \mathbf{k}_R and is separated from the lower (upper) dispersive band by a gap of $|\Delta|$ [Fig. 1(e)], which is just equal to the site-energy difference between sites A and B (C). There is also a flat band in the kagome lattice, where the flat band touches the upper dispersive band at the top.²⁶ On the LCS lattice, the flat band touches the upper dispersive band at the bottom (or the lower dispersive band at the top).

Let us focus attention on the vicinity of point R . By expanding the wave vector around \mathbf{k}_R as $\mathbf{k}=\mathbf{k}_R+\mathbf{q}$, up to the second order of q_x and q_y , the dispersion relation is reduced to $E_{\pm} = \pm \sqrt{m^2 v_0^4 + \hbar^2 q^2 v_0^2}$ with effective mass $m=|\Delta|/v_0^2$ and velocity $v_0=ta/\hbar$. It is a typical relativistic dispersion relation, in which the effective mass depends on the site-energy difference. Since the site-energy difference can be easily controlled by tuning the laser intensities, it is easy to realize a crossover from massive to massless Dirac fermions in the ultracold atomic system. The case of massless Dirac fermions is of particular interest, in which $E_{\pm} = \pm (\hbar q) v_0$. The energy of the fermions disperses linearly in the wave vector, which resembles the spectrum of the ultrarelativistic particles, and thus a Dirac cone is formed around the Dirac point \mathbf{k}_R . In what follows we focus on the massless Dirac fermions in the Dirac cone, for which Hamiltonian (2) can be reduced to

$$H_0 = \hbar v_0 \begin{pmatrix} 0 & q_x & 0 \\ q_x & 0 & q_y \\ 0 & q_y & 0 \end{pmatrix}. \quad (3)$$

Although Eq. (3) is derived from the nearest-neighbor tight-binding model, the flat band and the Dirac cone structure on the LCS lattice are protected by the symmetry of the lattice and will not be destroyed by the second or third nearest-neighbor hopping.

A striking feature of the massless Dirac fermions on the LCS lattice is the appearance of the single Dirac cone together with a flat band across the Dirac point, for there is only one inequivalent R point in the Brillouin zone. For the two-dimensional electron systems described by the Weyl equation, the Dirac points must come in pairs.⁸ As an example, there are two inequivalent Dirac cones in graphene.

The single Dirac cone here is quite different from that either in graphene or in the surface states of the topological insulators, because the present Dirac fermions do not satisfy the two-component Weyl equation, even though they have linear dispersion relation. Another important difference between graphene and the LCS lattice is whether or not there exists a Berry's phase enclosing the Dirac point. There is a π Berry's phase for the Dirac electrons in graphene and in the surface states of the topological insulators. Without the intervalley scattering, the π Berry's phase makes the Dirac fermions exhibit antilocalization behavior with disorder.²⁸ The occurrence of the π Berry's phase is a general result of two conical band touching.²⁹ On the LCS lattice, the Dirac point is a touching point for the three bands. After a proper unitary transformation, Hamiltonian (3) can be written as $H_0 = v_0 \mathbf{q} \cdot \mathbf{J}$, where \mathbf{J} is a pseudospin of the quantum number 1 with three eigenvalues. The pseudospin comes from the LCS crystal structure consisting of three sublattices. From this Hamiltonian, one finds that the massless Dirac fermions on the LCS lattice are the chiral particles of pseudospin-1. Since the matrix representations of the pseudospin and spin are the same, the Berry's phase acquired by the massless Dirac fermions here enclosing the Dirac point is equivalent to that acquired by the spin-1 particle in a rotational magnetic field, yielding a vanishing value (defined up to 2π).³⁰ The vanishing Berry's phase and the flat band across the Dirac point result from the three-component quantum equation for pseudospin-1 fermions.

For a magnetic field B , the Landau levels coming from the two dispersive bands are obtained as $E_n = \pm \sqrt{2n+1} \hbar \omega$, where $\hbar \omega = \hbar v_0 / l_B$ and $n=0, 1, 2, \dots$ with the magnetic length defined as $l_B = \sqrt{\hbar c / eB}$. This result is different from that either in the system of the nonrelativistic massive particles or in graphene. For the nonrelativistic case, the Landau levels are given by $E_n = (n+1/2) \hbar \omega_{nr}$ with $\hbar \omega_{nr} = \hbar^2 / (ml_B^2)$ depending on particle mass m . In graphene, the Landau levels are given by $E_n = \pm \sqrt{2n} \hbar \omega$ with the Landau level of $E=0$ induced by the π Berry's phase.³¹ It is expected that, due to the single Dirac cone and unique Landau levels, the quantum Hall effect on the LCS lattice could be more stable than in the conventional electron systems and could exhibit new features.

The massless Dirac fermions on the LCS lattice exhibit amazing transport properties such as the Klein tunneling.²⁷ For simplicity, we consider the particle tunneling through a rectangular potential barrier with potential $U(x) = U_0$ in the interval of $0 < x < D$ and zero elsewhere. Such a potential barrier was used to show the Klein tunneling in graphene.²⁷ Since the parallel wave vector, q_y , is conserved in the tunneling process, the wave function of the particle can be written as $\psi(x, y) = \psi(x) \exp(iq_y y)$. It is straightforward to solve $\psi(x)$ from Hamiltonian $H = H_0 + U(x)$ with H_0 given by Eq. (3). Consider a particle of energy $E > 0$ incident on the interface at $x=0$ from the left at an angle ϕ to the interface normal. The wave function is given by $\psi(x) = (\cos \phi \ 1 \ \sin \phi)^T \exp(iq_x x) + r (-\cos \phi \ 1 \ \sin \phi)^T \exp(-iq_x x)$ for $x < 0$, where r is the reflection amplitude, superscript T stands for the transpose of the matrix, $q_y = (E / \hbar v_0) \sin \phi$, and $q_x = [(E / \hbar v_0)^2 - q_y^2]^{1/2}$ is the perpendicular wave vector outside the barrier. The wave functions for $0 < x < D$ and x

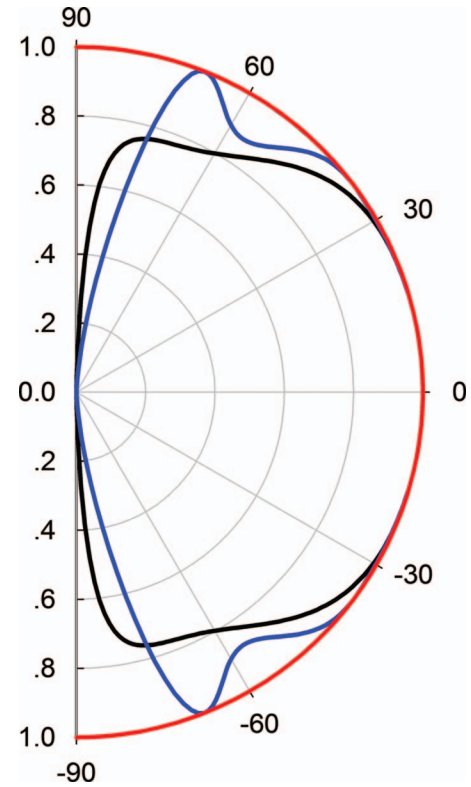


FIG. 2. (Color) The polar graph of transmission coefficient T as a function of incident angle ϕ . The energy of the incident particle is $0.3V_0$ (black curve), $0.4V_0$ (blue curve), and $0.5V_0$ (red curve), respectively, with $V_0 D / (\hbar v_0) = 40$.

$> D$ can also be easily found. By integrating the Schrödinger equation $H\psi(x) = E\psi(x)$ over the interval expanded in the vicinity of the interface, the boundary conditions are obtained. By matching the wave functions at boundaries $x=0$ and $x=D$, the transmission coefficient is obtained as

$$T = \frac{4u^2}{4u^2 + (1 - u^2)^2 \sin^2 k_x D}, \quad (4)$$

which is valid for arbitrary U_0 and D . Here, $k_x = s[(E - U_0)^2 / (\hbar v_0)^2 - q_y^2]^{1/2}$ is the wave vector inside the barrier with $s = \text{sgn}(E - U_0)$, and $u = \cos \phi / \cos \theta$ with $\theta = \arctan(q_y / k_x)$ as the refraction angle.

The angular dependence of transmission coefficient T is plotted in Fig. 2 for several energies with $V_0 D / (\hbar v_0) = 40$. From Eq. (4) and Fig. 2, one finds that $T=1$ for the normal incidence ($q_y=0$ and $u=1$) and so the barrier becomes perfectly transparent. This perfect tunneling can be understood by the conservation of the pseudospin of massless Dirac fermions and is similar to the Klein tunneling appeared in graphene.²⁷ Another similarity is the resonance tunneling of $T=1$ under conditions $q_x D = N\pi$ with N the integer, as shown by the blue line at $\phi \approx 70^\circ$ in Fig. 2. Owing to the three-component pseudospin of massless Dirac fermions, the Klein tunneling on the LCS lattice has its new feature. At $E = U_0/2$, k_x is always equal to $(-q_x)$ and $u=1$ in Eq. (4), regardless of ϕ so that the barrier becomes perfectly transparent ($T \equiv 1$) for all the incident angles. The all-angle per-

fect tunneling shown by the red curve in Fig. 2 is very distinctive and does not occur for the Dirac fermions in graphene. For $E \neq U_0/2$, although the barrier is not all-angle transparent, the transmission coefficient is still near 100% for rather large incident angles, as shown in Fig. 2. The nearly perfect transmission can occur in a larger range of ϕ on the LCS lattice compared with that in graphene, which can be understood by the following argument. In the high-barrier case of $E \ll U_0$, the transmission coefficient can be approximately obtained as $T(\phi) \approx 1 - \sin^2(q_x D) \phi^4/4$ for small ϕ . The present deviation from $T(\phi)=1$ is of the order of (ϕ^4) ,

while in graphene that deviation was found to be of the order of (ϕ^2) .²⁷ As a result, the Klein tunneling in a quite large range of incident angles on the LCS lattice, if realized in condensed matter, will be helpful in the electron optics such as lensing and focusing.^{32,33}

This work is supported by the National Natural Science Foundation of China under Grants No. 10504011 and No. 60825402, and also by the State Key Program for Basic Researches of China under Grants No. 2006CB921803, No. 2009CB929504, and No. 2010CB923401.

*shen@nju.edu.cn

- ¹K. S. Novoselov, D. Jiang, F. Schedin, T. J. Booth, V. V. Khotkevich, S. V. Morozov, and A. K. Geim, Proc. Natl. Acad. Sci. U.S.A. **102**, 10451 (2005).
- ²K. S. Novoselov, A. K. Geim, S. V. Morozov, D. Jiang, Y. Zhang, S. V. Dubonos, I. V. Grigorieva, and A. A. Firsov, Science **306**, 666 (2004).
- ³K. S. Novoselov, A. K. Geim, S. V. Morozov, D. Jiang, M. I. Katsnelson, I. V. Grigorieva, S. V. Dubonos, and A. A. Firsov, Nature (London) **438**, 197 (2005).
- ⁴Y. B. Zhang, Y. W. Tan, H. L. Stormer, and P. Kim, Nature (London) **438**, 201 (2005).
- ⁵A. K. Geim and K. S. Novoselov, Nature Mater. **6**, 183 (2007).
- ⁶A. H. Castro Neto, F. Guinea, N. M. R. Peres, K. S. Novoselov, and A. K. Geim, Rev. Mod. Phys. **81**, 109 (2009).
- ⁷T. Ando, T. Nakanishi, and R. Saito, J. Phys. Soc. Jpn. **67**, 2857 (1998).
- ⁸H. B. Nielsen and M. Ninomiya, Phys. Lett. **130B**, 389 (1983).
- ⁹L. Fu, C. L. Kane, and E. J. Mele, Phys. Rev. Lett. **98**, 106803 (2007).
- ¹⁰L. Fu and C. L. Kane, Phys. Rev. B **76**, 045302 (2007).
- ¹¹J. E. Moore and L. Balents, Phys. Rev. B **75**, 121306(R) (2007).
- ¹²Y. Xia, D. Qian, D. Hsieh, L. Wray, A. Pal, H. Lin, A. Bansil, D. Grauer, Y. S. Hor, R. J. Cava, and M. Z. Hasan, Nat. Phys. **5**, 398 (2009).
- ¹³H. J. Zhang, C. X. Liu, X. L. Qi, X. Dai, Z. Fang, and S. C. Zhang, Nat. Phys. **5**, 438 (2009).
- ¹⁴I. Bloch, Nat. Phys. **1**, 23 (2005).
- ¹⁵J. R. Anglin and W. Ketterle, Nature (London) **416**, 211 (2002).
- ¹⁶M. Lewenstein, A. Sanpera, V. Ahufinger, B. Damski, A. Sen(De), and U. Sen, Adv. Phys. **56**, 243 (2007).
- ¹⁷I. Bloch, J. Dalibard, and W. Zwerger, Rev. Mod. Phys. **80**, 885 (2008).
- ¹⁸D. Jaksch, C. Bruder, J. I. Cirac, C. W. Gardiner, and P. Zoller, Phys. Rev. Lett. **81**, 3108 (1998).
- ¹⁹L. M. Duan, E. Demler, and M. D. Lukin, Phys. Rev. Lett. **91**, 090402 (2003).
- ²⁰M. Greiner, O. Mandel, T. Esslinger, T. W. Hänsch, and I. Bloch, Nature (London) **415**, 39 (2002).
- ²¹M. A. Baranov, K. Osterloh, and M. Lewenstein, Phys. Rev. Lett. **94**, 070404 (2005).
- ²²S. L. Zhu, H. Fu, C. J. Wu, S. C. Zhang, and L. M. Duan, Phys. Rev. Lett. **97**, 240401 (2006).
- ²³J. Y. Vaishnav, J. Ruseckas, C. W. Clark, and G. Juzelunas, Phys. Rev. Lett. **101**, 265302 (2008).
- ²⁴S. L. Zhu, B. G. Wang, and L. M. Duan, Phys. Rev. Lett. **98**, 260402 (2007).
- ²⁵C. J. Wu, D. Bergman, L. Balents, and S. Das Sarma, Phys. Rev. Lett. **99**, 070401 (2007).
- ²⁶D. L. Bergman, C. J. Wu, and L. Balents, Phys. Rev. B **78**, 125104 (2008).
- ²⁷M. I. Katsnelson, K. S. Novoselov, and A. K. Geim, Nat. Phys. **2**, 620 (2006).
- ²⁸H. Suzuura and T. Ando, Phys. Rev. Lett. **89**, 266603 (2002).
- ²⁹G. P. Mikitik and Y. V. Sharlai, Phys. Rev. Lett. **82**, 2147 (1999).
- ³⁰M. V. Berry, Proc. R. Soc. London, Ser. A **392**, 45 (1984).
- ³¹Y. Zheng and T. Ando, Phys. Rev. B **65**, 245420 (2002).
- ³²H. van Houten and C. W. J. Beenakker, in *Analogies in Optics and Micro Electronics*, edited by W. van Haeringen and D. Lenstra (Kluwer, New York, 1990).
- ³³V. V. Cheianov, V. Fal'ko, and B. L. Altshuler, Science **315**, 1252 (2007).